ELSEVIER

Volume 180, Number 12, December 2007

JOURNAL OF SOLID STATE CHEMISTRY

www.elsevier.com/locate/jssc

CONTENTS

Abstracted/indexed in BioEngineering Abstracts, Chemical Abstracts, Coal Abstracts, Current Contents/Physics, Chemical, & Earth Sciences, Engineering Index, Research Alert, SCISEARCH, Science Abstracts, and Science Citation Index. Also covered in the abstract and citation database SCOPUS®. Full text available on ScienceDirect®.

Regular Articles

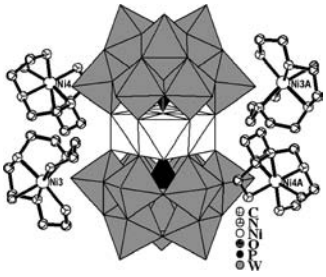

Three inorganic–organic composite sandwich-type phosphotungstates $[Ni(tepa)(H_2O)]_4H_2[Ni_4(H_2O)_2(\alpha\text{-}B\text{-}PW_9O_{34})_2]\cdot 8\ H_2O$ (**1**), $(enH_2)_3[Ni_2(H_2O)_{10}][Ni_4(H_2O)_2(\alpha\text{-}B\text{-}PW_9O_{34})_2]\cdot en\cdot 8H_2O$ (**2**) and $(enH_2)_{10}[Mn_4(H_2O)_2(\alpha\text{-}B\text{-}PW_9O_{34})_2]_2\cdot 20H_2O$ (**3**) have been hydrothermally synthesized and structurally characterized by IR spectra, elemental analysis, thermogravimetric analysis and magnetic susceptibility. They all contain tetra-*M* sandwiched polyoxoanions $[M_4(H_2O)_2(\alpha\text{-}B\text{-}PW_9O_{34})_2]^{10-}$ ($M=Ni^{2+}$ or Mn^{2+}) and nickel-organoamine cations or organoamine cations work as the charge balance ions.

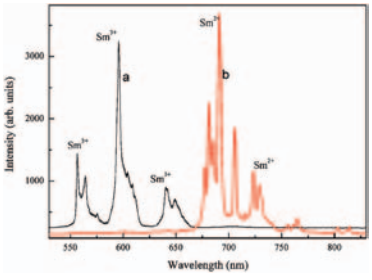

The Sm doped in $BaBPO_5$ as-prepared in air contains only Sm^{3+} ions and shows its fluorescence bands due to the $^4G_{5/2}$ to $^6H_{5/2}$, $^6H_{7/2}$, $^6H_{9/2}$, and $^6H_{11/2}$ transitions (a) under the excitation of 488 nm Ar^+-ion laser. The emission spectra of the samples after X-ray subsequentially irradiations are characteristic of Sm^{2+} transitions between the energy levels of $4f^6$ electronic configurations (b). It is found that the conversion of $Sm^{3+}\rightarrow Sm^{2+}$ is very efficient in $BaBPO_5$ hosts after X-ray irradiation.

Regular Articles—Continued

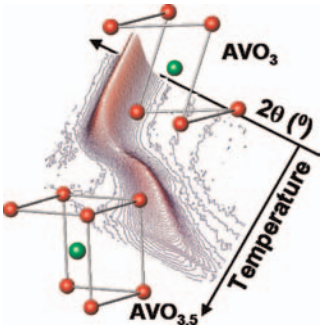

Topotactic oxidation of AVO_3 bixbyite to $AVO_{3.5}$ defect fluorite structure followed by in-situ powder X-ray diffraction. The upper structural diagram shows a six coordinated (A/V)-O_6 fragment in bixbyite, the lower structure illustrates the same seven-fold coordinated (A/V)-O_7 cubic environment in the defect fluorite structure.

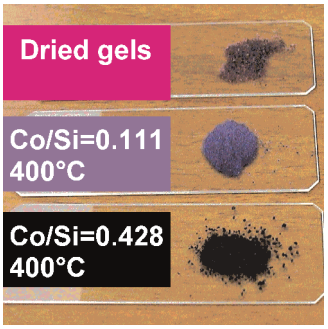

Highly dispersed cobalt–silicon mixed oxide nanocomposites (Co/Si = 0.111, 0.250 and 0.428) were obtained by a modified sol–gel method using almost solely aqueous solutions. The nature of cobalt species and their interactions with the siloxane matrix are strongly depending on both the cobalt loading and the heat treatment. All materials retained high surface areas also after treatments at 600 °C and exhibited surface Lewis acidity.

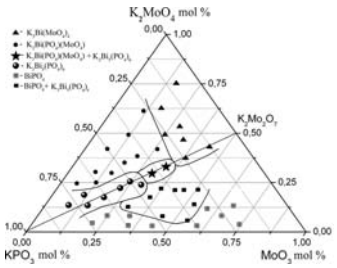

Composition diagram of the K_2MoO_4–KPO_3–MoO_3 system containing 15 mol% Bi_2O_3 with approximate fields of phase formation bismuth phosphates, molybdate and phosphate-molybdate.

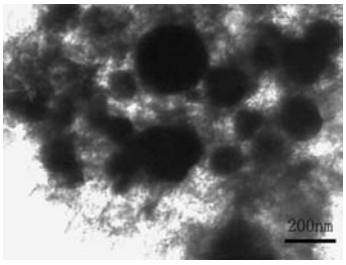

The amorphous carbon coating on the Sn–Sb particles was prepared from aqueous glucose solutions using a hydrothermal method. Because the outer layer carbon of composite materials is loose cotton-like and porous-like, it can accommodate the expansion and contraction of active materials to maintain the stability of the structure, and hinder effectively the aggregation of nano-sized alloy particles.

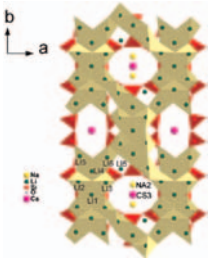

Li_2O-layers formed by edge- and corner-sharing LiO_4- and LiO_3-moieties in the zeolite-like lithosilicate RUB-29 provide optimal pathways for conducting Li^+. The number of empty Li sites in this layer-like configuration could increase via 'simple' Na^+-exchange processes, promoting fast Li motions.

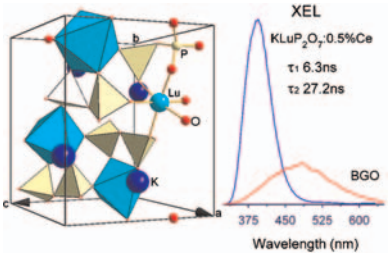

The perspective view of $KLuP_2O_7$ unit cell. The crystal structures of five $AREP_2O_7$ diphosphates were obtained from Rietveld refinement. Under the excitation of hard X-ray, the Ce^{3+}-activated $AREP_2O_7$ (A = Na–Cs; RE = Y, Lu) feature strong Ce^{3+} 5*d*–4*f* emission with high light yield (1–2 times of that of $Bi_4Ge_3O_{12}$) and fast decay time within 20–28 ns.

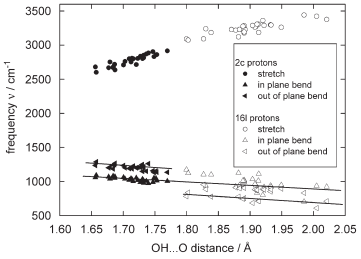

The characteristic O–H vibrational modes of $Ba_2In_2O_4(OH)_2$ as a function of the OH···O hydrogen bond length.

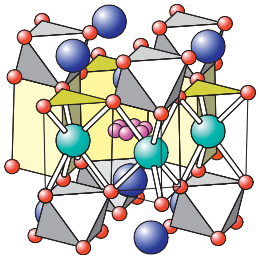

Hexagonal perovskites of the $[A'_2O_{1+\delta}][A_nB_{n-1}O_{3n}]$ family have so far only been known for the transition metals Mn, Nb, Ru, and Ir. In this paper, three new $n = 2$ examples containing platinum as *B*-type cation are presented. The structure and physical properties of the three title compounds were investigated by XRD Rietveld refinements, thermogravimetry, X-ray absorption spectroscopy, magnetic measurements and optical spectroscopy.

Continued

Magnetic and Mössbauer studies of 5% Fe-doped $BiMnO_3$
Alexei A. Belik, Naoaki Hayashi, Masaki Azuma, Shigetoshi Muranaka, Mikio Takano and Eiji Takayama-Muromachi
page 3401

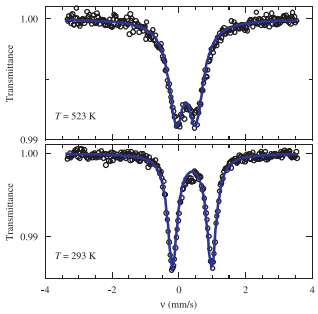

Mössbauer spectra of $BiMn_{0.95}Fe_{0.05}O_3$ at 523 and 293 K.

High-pressure structural evolution of a perovskite solid solution $(La_{1-x},Nd_x)GaO_3$
R.J. Angel, J. Zhao, N.L. Ross, C.V. Jakeways, S.A.T. Redfern and M. Berkowski
page 3408

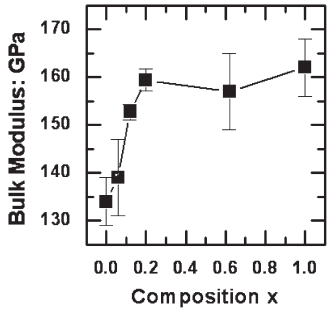

High-pressure structure determinations of six perovskites on the $La_{1-x}Nd_xGaO_3$ join show that at La-rich compositions the GaO_6 octahedra have much lower bulk moduli, as shown in the figure. This softening of the octahedra drives the high-pressure phase transition from *Pbnm* to *R-3c* structures.

Effect of electrolysis conditions on photocatalytic activities of the anodized TiO_2 films
Kinji Onoda and Susumu Yoshikawa
page 3425

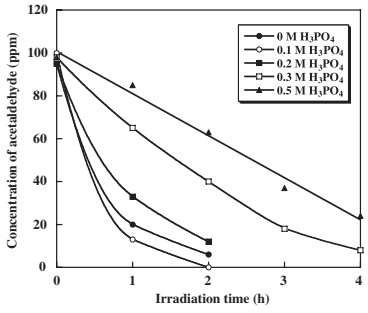

The effect of concentration of H_3PO_4 on the photocatalytic activity of the anodized TiO_2 films was investigated. The pre-nitrided titanium plates were anodized in electrolyte of 1.5 M H_3PO_4 and 0.3 M H_2O_2 with varying H_3PO_4 concentration in the range from 0 to 0.5 M. The highest photocatalytic activity was obtained at H_3PO_4 concentration of 0.1 M.

Synthesis of Cd/(Al + Fe) layered double hydroxides and characterization of the calcination products
M.R. Pérez, C. Barriga, J.M. Fernández, V. Rives and M.A. Ulibarri
page 3434

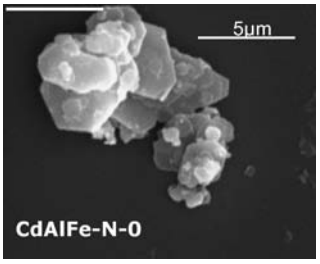

Layered double hydroxides (LDHs) containing Cd(II), Al(III), and Fe(III) in the brucite-like layers with different starting Fe/Al atomic ratios and with nitrate as counteranion have been prepared following the coprecipitation method. An additional Cd(II),Al(III)-LDH sample interlayered with hexacyanoferrate(III) ions has been prepared by ionic exchange. Calcination at 800 °C shows diffraction lines corresponding to CdO and to spinel-type materials.

Synthesis and characterization of nanoparticulate MnS within the pores of mesoporous silica
Louse Barry, Mark Copley, Justin D. Holmes, David J. Otway, Olga Kazakova and Michael A. Morris
page 3443

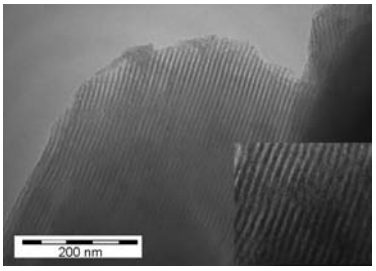

A novel manganese ethylxanthate precursor was used to impregnate the pore network of mesoporous silica and was decomposed to yield MnS particles smaller or equal to the pore size. The particles exhibit all three common polymorphs, demonstrate unexpected ferromagnetism at low temperatures and display a strong luminescence.

Photoluminescence properties of $La(PO_3)_3:Tb^{3+}$ under VUV excitation
Yuhua Wang and Dan Wang
page 3450

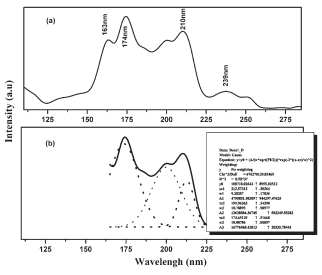

A strongest band around 174nm, observed in the excitation spectrum of $La_{0.55}(PO_3)_3:Tb^{3+}_{0.45}$, indicates that $La_{0.55}(PO_3)_3:Tb^{3+}_{0.45}$ can efficiently absorb the vacuum ultraviolet (VUV) energy. The band overlapping around 210 nm implies that the excited energy can be efficiently transferred from VUV to UV region. Therefore, $La_{0.55}(PO_3)_3:Tb^{3+}_{0.45}$ is a promising phosphor in VUV region.

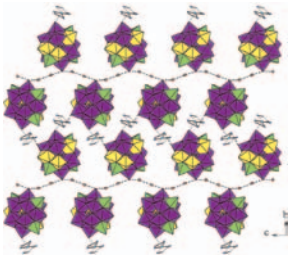

A novel complex $[Cu(phen)_2]_3\{PW_4^{VI}W_5^{V}V_3^{IV}O_{40}(V^{IV}O)_3[Cu(en)_2]\}\cdot 4H_2O$, the first example of tri-capped and mono-supported highly reduced pseudo-Keggin-type tungstovanadophosphate was synthesized under hydrothermal condition. And the heteropolyanions are linked by water dimer and cation $[Cu(phen)_2]^{2+}$ through the hydrogen bond forming a three-dimensional (3D) supramolecular network. Interestingly, the water dimer and terminal oxygen of the polyanion cluster constitute a beautiful supramolecular helix chain.

Crystals of the mixed-valent compound $(Bi_6O_5)Rh_8^{3+}Rh_4^{4+}O_{24}$ show semiconducting properties, and magnetic susceptibility data indicate a localized moment for Rh^{4+}. Structure refinements at 173 and 296 K show partial charge ordering between Rh^{3+} and Rh^{4+}.

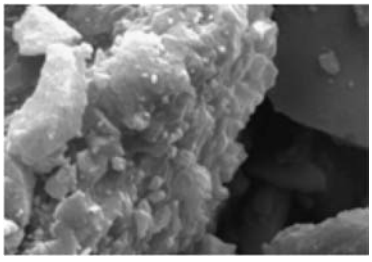

$Ni(OH)_2$ solid precursors can be readily selected on the basis of their defects, themselves stemming from the nickel salt chosen for precipitation, to rapidly synthesize neutral Ni(II)–aminoacid complexes by ligand-promoted dissolution.

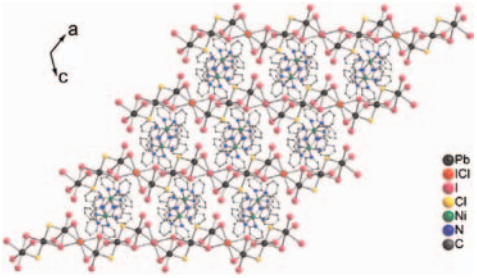

Based upon magnetic metal-organic complex as template, a novel one-dimensional haloplumbate containing mixed-halide anion has been successfully synthesized. Its structural characteristics, optical bandgap, magnetic and thermal properties are reported.

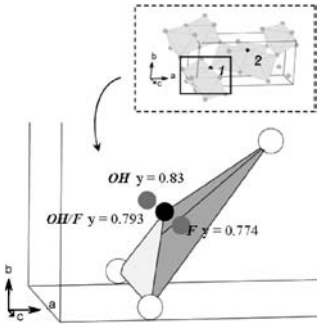

Representation of the splitting of site 1 (black sphere) into two positions (grey spheres) corresponding respectively to the presence of hydroxyl or fluoride ions.

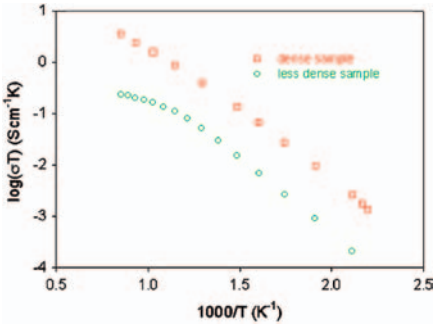

Total conductivity of $BaZr_{0.8}Y_{0.2}O_{3-\delta}$ samples in wet 5% H_2/Ar with (red) and without (green) addition of 1 wt% ZnO.

Continued

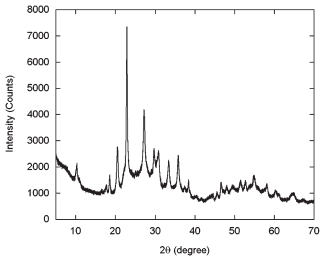

The formation of $ZrW_2O_7(OH)_2 \cdot 2H_2O$ shows a strong dependence on reaction conditions. Both acid concentration and acid counter-ion play a significant role in the crystallization. High temperatures, high acid concentrations, and the presence of chloride or bromide ions promote the formation of well-crystallized $ZrW_2O_7(OH)_2 \cdot 2H_2O$. For low acid concentrations, a new zirconium tungstate hydrate polymorph is observed.

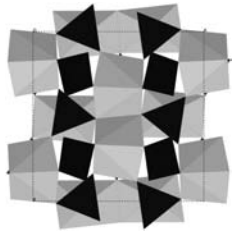

Yttrium molybdate ($Y_2Mo_3O_{12}$) prepared by non-hydrolytic sol–gel chemistry crystallizes in a mixture of orthorhombic polymorphs with different atomic connectivities. The *Pbcn* and *Pba*2 phases coexist over a narrow temperature range. Crystallization of the *Pbcn* structure is kinetically favored. The *Pba*2 polymorph is the thermodynamically stable phase at low temperatures, and converts to *Pbcn* above 550 °C.

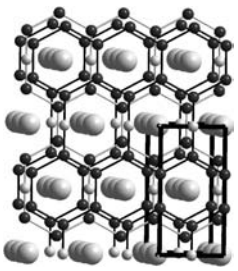

Dy_2B_4C crystallizes a new structure type where planar 6^3-Dy metal atom layers alternate with planar non-metal layers consisting of ribbons of fused B_6 hexagons bridged by carbon atoms. Isostructural analogues with Tb, Ho and Er have also been characterized.

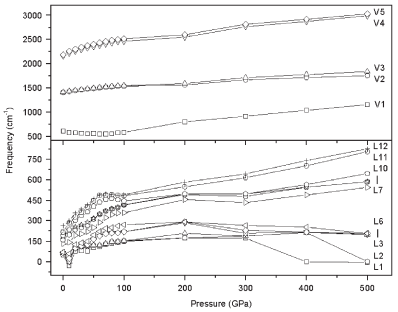

Silver azide attracts scientific and technological interest as an energetic material. There are sufficient difficulties to study it experimentally at extreme conditions due to their explosive nature. This paper presents a detailed first-principles study of the structural and vibrational properties of crystalline silver azide under hydrostatic pressure of 0–500 GPa.

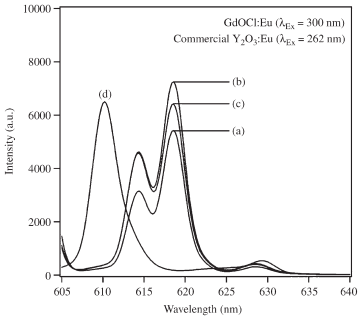

Three different synthetic methods were explored to synthesize *Ln*OCl:Eu (*Ln* = La and Gd) phosphors. The application of solvothermal technique was very effective to selectively control the particle shape and consequently to enhance the luminescence intensity if we use an appropriate surfactant material.

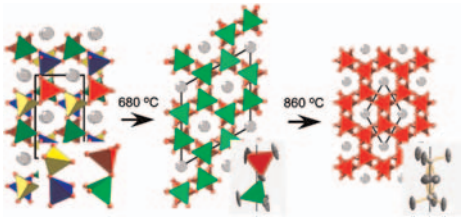

$SrAl_2O_4$ crystal structure evolution through the phase transitions between $P2_1$, $P6_3(\sqrt{3}A)$, and $P6_322$ modifications. Insets show displacements of apical oxygen atoms linking tridymite-type layers.

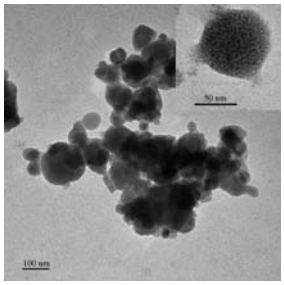

TEM image of magnetite/poly(thiophene) nanocomposite.

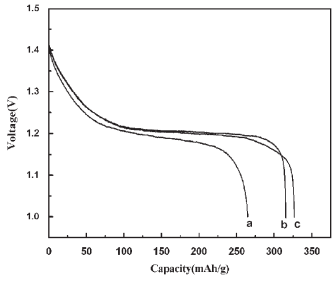

β-$Ni(OH)_2$ nanorods, NiO sub-microtubes, Ni nanospheres and flower-like nickel complexes nanostructures were synthesized using the $NiC_2O_4 \cdot 2H_2O$ nanorods precursor, which were fabricated via the microemulsion-mediated solvothermal synthesis method. The synthesized β-$Ni(OH)_2$ nanorods composed of fine nanosheets shown excellent electrochemical performance as an electrode material in rechargeable battery systems.

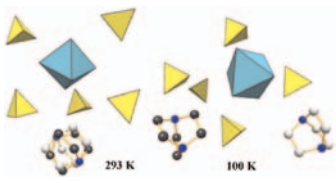

The new dabcodiium hexaaquairon(II) bis(sulfate), $(C_6H_{14}N_2)[Fe(H_2O)_6](SO_4)_2$, was prepared and characterized. It exhibits a supramolecular structure and undergoes a reversible order–disorder phase transition at −2.3 °C.

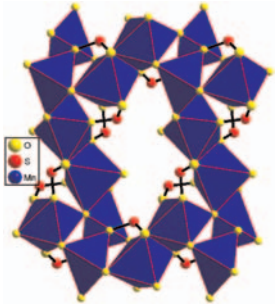

A three-dimensional manganese sulfite with one-dimensional channels showing selective hydrogen absorption has been synthesized and characterized.

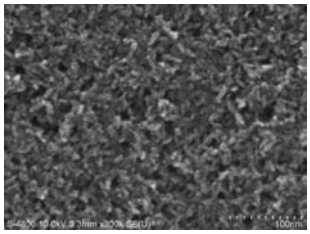

Carbon modifying not only produces homogeneous worm-like structure with uniform pores, but also extends the absorbance spectra of the as-prepared titania films into visible region.

Rapid Communications

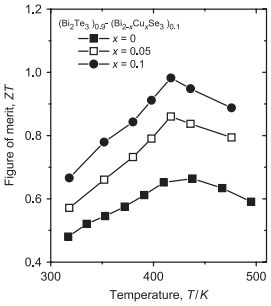

After Cu-doping with $x = 0.1$, the highest ZT value of 0.98 is obtained at 417 K, which is about 0.32 and 0.12 higher than those of Cu-free $Bi_2Se_{0.3}Te_{2.7}$ and the Ag-doped alloys $(Bi_2Te_3)_{0.9}$–$(Bi_{2-x}Ag_xSe_3)_{0.1}$ ($x = 0.4$), respectively.

Continued

Fabrications of some kinds of 2-D frameworks consisting of nanosized polyoxomolybdate anion $[Mo_{36}O_{112}(H_2O)_{16}]^{8-}$ via condensation processes

Kazuo Eda, Yuichi Iriki, Kenjiro Kawamura, Takeshi Ikuki and Masahiko Hayashi

page 3588

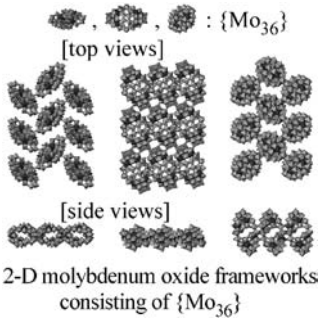

The image shows a variety of 2-D molybdenum oxide frameworks consisting of nanosized polyoxometalate anion $[Mo_{36}O_{112}(H_2O)_{16}]^{8-}$ ($\{Mo_{36}\}$), obtained by our fabrication techniques. The variations are expected to provide diversity in physical properties of the frameworks.

Author inquiries

Submissions

For detailed instructions on the preparation of electronic artwork, consult the journal home page at http://authors.elsevier.com.

Other inquiries

Visit the journal home page (http://authors.elsevier.com) for the facility to track accepted articles and set up e-mail alerts to inform you of when an article's status has changed. The journal home page also provides detailed artwork guidelines, copyright information, frequently asked questions and more.

Contact details for questions arising after acceptance of an article, especially those relating to proofs, are provided after registration of an article for publication.

Language Polishing

Authors who require information about language editing and copyediting services pre- and post-submission should visit http://www.elsevier.com/wps/find/authorshome.authors/languagepolishing or contact authorsupport@elsevier.com for more information. Please note Elsevier neither endorses nor takes responsibility for any products, goods, or services offered by outside vendors through our services or in any advertising. For more information please refer to our Terms & Conditions at http://www.elsevier.com/wps/find/termsconditions.cws_home/termsconditions.

For a full and complete Guide for Authors, please refer to *J. Solid State Chem.,* Vol. 180, Issue 1, pp. *bmi–bmv*. The instructions can also be found at http://www.elsevier.com/wps/find/journaldescription.cws_home/622898/authorinstructions.

Journal of Solid State Chemistry has no page charges.